The Astrophysical Journal Letters, 941:L27 (8pp), 2022 December 20 https://doi.org/10.3847/2041-8213/aca674

PHANGS-JWST First Results: Spurring on Star Formation: JWST Reveals Localized Star Formation in a Spiral Arm Spur of NGC 628

Thomas G. Williams[1,2], Jiayi Sun[3,4,32], Ashley T. Barnes[5], Eva Schinnerer[2], Jonathan D. Henshaw[2,6], Sharon E. Meidt[7], Miguel Querejeta[8], Elizabeth J. Watkins[9], Frank Bigiel[5], Guillermo A. Blanc[10,11], Médéric Boquien[12], Yixian Cao[13], Mélanie Chevance[14,15], Oleg V. Egorov[9], Eric Emsellem[16,17], Simon C. O. Glover[14], Kathryn Grasha[18], Hamid Hassani[19], Sarah Jeffreson[20], María J. Jiménez-Donaire[8], Jaeyeon Kim[14], Ralf S. Klessen[14,21], Kathryn Kreckel[9], J. M. Diederik Kruijssen[15], Kirsten L. Larson[22], Adam K. Leroy[23,24], Daizhong Liu[13], Ismael Pessa[2,25], Jérôme Pety[26,27], Francesca Pinna[2], Erik Rosolowsky[19], Karin M. Sandstrom[28], Rowan Smith[29], Mattia C. Sormani[14], Sophia Stuber[2], David A. Thilker[30], and Bradley C. Whitmore[31]

[1] Sub-department of Astrophysics, Department of Physics, University of Oxford, Keble Road, Oxford OX1 3RH, UK; williams@mpia.de
[2] Max-Planck-Institut für Astronomie, Königstuhl 17, D-69117, Heidelberg, Germany
[3] Department of Physics and Astronomy, McMaster University, Hamilton, ON L8S 4M1, Canada
[4] Canadian Institute for Theoretical Astrophysics (CITA), University of Toronto, 60 St George Street, Toronto, ON M5S 3H8, Canada
[5] Argelander-Institut für Astronomie, Universität Bonn, Auf dem Hügel 71, D-53121, Bonn, Germany
[6] Astrophysics Research Institute, Liverpool John Moores University, 146 Brownlow Hill, Liverpool L3 5RF, UK
[7] Sterrenkundig Observatorium, Universiteit Gent, Krijgslaan 281 S9, B-9000 Gent, Belgium
[8] Observatorio Astronómico Nacional (IGN), C/Alfonso XII, 3, E-28014 Madrid, Spain
[9] Astronomisches Rechen-Institut, Zentrum für Astronomie der Universität Heidelberg, Mönchhofstraße 12-14, D-69120 Heidelberg, Germany
[10] The Observatories of the Carnegie Institution for Science, 813 Santa Barbara Street, Pasadena, CA, USA
[11] Departamento de Astronomía, Universidad de Chile, Camino del Observatorio 1515, Las Condes, Santiago, Chile
[12] Centro de Astronomía (CITEVA), Universidad de Antofagasta, Avenida Angamos 601, Antofagasta, Chile
[13] Max-Planck-Institut für extraterrestrische Physik, Giessenbachstraße 1, D-85748 Garching, Germany
[14] Universität Heidelberg, Zentrum für Astronomie, Institut für theoretische Astrophysik, Albert-Ueberle-Str. 2, D-69120 Heidelberg, Germany
[15] Cosmic Origins of Life (COOL) Research DAO, coolresearch.io.
[16] European Southern Observatory, Karl-Schwarzschild-Straße 2, D-85748 Garching, Germany
[17] Univ Lyon, Univ Lyon1, ENS de Lyon, CNRS, Centre de Recherche Astrophysique de Lyon UMR5574, F-69230 Saint-Genis-Laval France
[18] Research School of Astronomy and Astrophysics, Australian National University, Canberra, ACT 2611, Australia
[19] Department of Physics, University of Alberta, Edmonton, Alberta, T6G 2E1, Canada
[20] Center for Astrophysics, Harvard & Smithsonian, 60 Garden Street, Cambridge, MA, USA
[21] Universität Heidelberg, Interdisziplinäres Zentrum für Wissenschaftliches Rechnen, Im Neuenheimer Feld 205, D-69120 Heidelberg, Germany
[22] AURA for the European Space Agency (ESA), Space Telescope Science Institute, 3700 San Martin Drive, Baltimore, MD 21218, USA
[23] Department of Astronomy, The Ohio State University, 140 West 18th Avenue, Columbus, Ohio 43210, USA
[24] Center for Cosmology and Astroparticle Physics, 191 West Woodruff Avenue, Columbus, OH 43210, USA
[25] Leibniz-Institut für Astrophysik Potsdam (AIP), An der Sternwarte 16, D-14482 Potsdam, Germany
[26] IRAM, 300 rue de la Piscine, F-38400 Saint Martin d'Hères, France
[27] LERMA, Observatoire de Paris,PSL Research University, CNRS, Sorbonne Universités, F-75014 Paris, France
[28] Department of Physics, University of California, San Diego, 9500 Gilman Drive, San Diego, CA 92093, USA
[29] Jodrell Bank Centre for Astrophysics, Department of Physics and Astronomy, University of Manchester, Oxford Road, Manchester M13 9PL, UK
[30] Department of Physics and Astronomy, The Johns Hopkins University, Baltimore, MD 21218, USA
[31] Space Telescope Science Institute, 3700 San Martin Drive, Baltimore, MD, USA
Received 2022 October 21; revised 2022 November 28; accepted 2022 November 28; published 2022 December 16

Abstract

We combine JWST observations with Atacama Large Millimeter/submillimeter Array CO and Very Large Telescope MUSE Hα data to examine off-spiral arm star formation in the face-on, grand-design spiral galaxy NGC 628. We focus on the northern spiral arm, around a galactocentric radius of 3–4 kpc, and study two spurs. These form an interesting contrast, as one is CO-rich and one CO-poor, and they have a maximum azimuthal offset in MIRI 21 μm and MUSE Hα of around 40° (CO-rich) and 55° (CO-poor) from the spiral arm. The star formation rate is higher in the regions of the spurs near spiral arms, but the star formation efficiency appears relatively constant. Given the spiral pattern speed and rotation curve of this galaxy and assuming material exiting the arms undergoes purely circular motion, these offsets would be reached in 100–150 Myr, significantly longer than the 21 μm and Hα star formation timescales (both < 10 Myr). The invariance of the star formation efficiency in the spurs versus the spiral arms indicates massive star formation is not only triggered in spiral arms, and cannot simply occur in the arms and then drift away from the wave pattern. These early JWST results show that in situ star formation likely occurs in the spurs, and that the observed young stars are not simply the "leftovers" of stellar birth

[32] CITA National Fellow.

in the spiral arms. The excellent physical resolution and sensitivity that JWST can attain in nearby galaxies will well resolve individual star-forming regions and help us to better understand the earliest phases of star formation.

Unified Astronomy Thesaurus concepts: Galaxies (573); Spiral galaxies (1560); Interstellar medium (847); Star formation (1569)

1. Introduction

Spiral arms are a distinctive characteristic of star-forming galaxies, featuring large, curved arcs across the galaxy disks as gas is compressed and star formation occurs. Historically, spiral arms have been seen as the sites where the majority of stars form within galaxies (e.g., Morgan et al. 1953; Roberts 1969; Louie et al. 2013). This is thought to stem from high gas densities achieved in the spiral arms, combined with low shear (Elmegreen 2007), which favors cloud (and from this, star) formation (see reviews by Dobbs & Baba 2014; Chevance et al. 2022). Star formation triggering is also thought to take place in spiral arms, given the shocking that occurs at these locations (Roberts 1969), and the potential for cloud–cloud collisions (e.g., Kennicutt 1998; Tan 2000; Longmore et al. 2014; Chevance et al. 2020; Fukui et al. 2021). Here, gas compressed by molecular clouds colliding can lead to an episode of star formation.

Modern views of the process of star formation in spiral arms built from observations and simulations emphasize that the pattern of star formation in and around these locations is complex (e.g., Dobbs & Pringle 2010; Chandar et al. 2017; Schinnerer et al. 2017; Kim et al. 2020). This is thought to reflect that spiral arms are not smooth, singular structures but instead themselves host a complex array of substructures. These structures have a variety of names, such as spurs or feathers (see La Vigne et al. 2006, for a discussion of the nomenclature). These features protrude from the spiral arms, are fairly regularly spaced with azimuth, and are predicted in simulations to extend to kiloparsec scales. The origin of these spurs is currently unclear. Several mechanisms have been proposed, including gravitational instabilities (e.g., Dobbs & Bonnell 2006), magneto-Jeans instabilities (e.g., Kim & Ostriker 2006), wiggle instabilities (e.g., Wada & Koda 2004; Mandowara et al. 2022), supernova feedback, or formation on the edges of superbubbles (primarily feedback driven expansions of gas; see, e.g., Oey & Clarke 1997; Kim et al. 2020). Depending on the formation mechanism, these spurs are also thought to be viable sites of further fragmentation and collapse. Thus, star formation may not occur exclusively in the high-density spiral arm ridge. Measuring the star formation as a function of distance from spiral arms is critical for testing spur formation pathways, and can help us to better understand star formation associated with the spiral arm passage of gas.

Spurs can be seen in molecular gas tracers (Corder et al. 2008; Koda et al. 2009; Schinnerer et al. 2017; Stuber et al. 2022), as well as in the dust morphology (La Vigne et al. 2006). The goal of this work is to ask and answer whether stars are forming natively within spurs or if stars have formed in the dense spiral ridge and drifted to their present positions coincident with the spurs. Certainly for M51, the former appears to be the case (Schinnerer et al. 2017), as typical extragalactic star formation rate (SFR) tracers (Hα, 24 μm) are coincident with CO in the spurs, rather than with the ridge of the CO spiral arm. Localizing the natal site of star formation requires the use of a tracer of the youngest, most embedded phase of the star formation process (i.e., with timescales $<$10 Myr). This ensures that we can catch star formation "in the act." For this, the mid- and far-infrared are ideal, as bright and compact emission at these wavelengths directly traces the hot dust heated by young, embedded stars. However, given the limited resolution of the Spitzer MIPS (Rieke et al. 2004) instrument (which had a resolution of $\sim$300 pc at a distance of 10 Mpc, but was the only viable instrument in this wavelength range before JWST), until now localizing the mid-infrared (MIR) emission to spurs or spiral arms has been challenging in galaxies outside the Local Group. This means establishing whether the phenomenon of star formation within spurs is unique to M51 or a general feature of all disk galaxies is still an open question, with important implications for star formation models.

In this Letter, we use new JWST observations taken as part of the PHANGS-JWST Treasury Program (PI J. C. Lee; Lee et al. 2022) to study star formation in the spiral arms of NGC 628. We test whether star formation off of the spiral arms in NGC 628 could be from stars forming within spiral arms and then drifting, or whether stars are formed locally within spurs. The structure of this Letter is as follows: we briefly describe why NGC 628 is an ideal target for this study, and the data provenance in Section 2, and we identify our spiral arm region of interest and the timescales for offset between the spiral arm and spur in Section 3. We conclude in Section 4.

2. NGC 628 and Data

As an archetypal grand-design spiral galaxy, NGC 628 is an ideal target for studies of spiral arms, given its clear arm structure and lack of a bar. Located at a distance of 9.84 Mpc (McQuinn et al. 2017; Anand et al. 2021a, 2021b), NGC 628 is almost face-on ($i = 8.^{\circ}9$; Lang et al. 2020), and aligned nearly north-up with a position angle of $20.^{\circ}7$ (Lang et al. 2020). It is also the only galaxy in PHANGS-MUSE with a robustly measured spiral arm pattern speed from stellar kinematics by Williams et al. (2021; the rest of the pattern speeds in this work being attributed to bars), which is necessary to obtain timescales for the spur offset (Section 3). We present a three-color composite image in Figure 1 including the data we will use in this study, and Figure 2 presents a more holistic overview of the spurs, which shows the wealth of high-quality observations, and rich detail present in the PHANGS (and especially the PHANGS-JWST) data that exist for this galaxy. Returning to Figure 1, in blue, we show a CO($J = 2 - 1$), hereafter CO, moment 0 map from the Atacama Large Millimeter/submillimeter Array (ALMA; Leroy et al. 2021a, 2021b), tracing the cold molecular gas across the galactic disk. Here, a number of gas spurs are visible as structures that are almost perpendicular to the spiral arm. These data have a resolution of $\sim$1″ ($\sim$50 pc) and a sensitivity of $\sim$1 K km s^{-1}. In green, we show Hα emission from Very Large Telescope (VLT) MUSE observations as part of PHANGS-MUSE (Emsellem et al. 2022), tracing young stars that are producing ionizing radiation but have blown a hole in their natal cloud. The MUSE data also have a resolution of around 1″, with an Hα sensitivity of $\sim 1.5 \times 10^{37}$ erg s^{-1} kpc^{-2}. Hα emission traces star formation over timescales of $<$10 Myr (e.g., Moustakas et al. 2006; Kennicutt & Evans 2012;

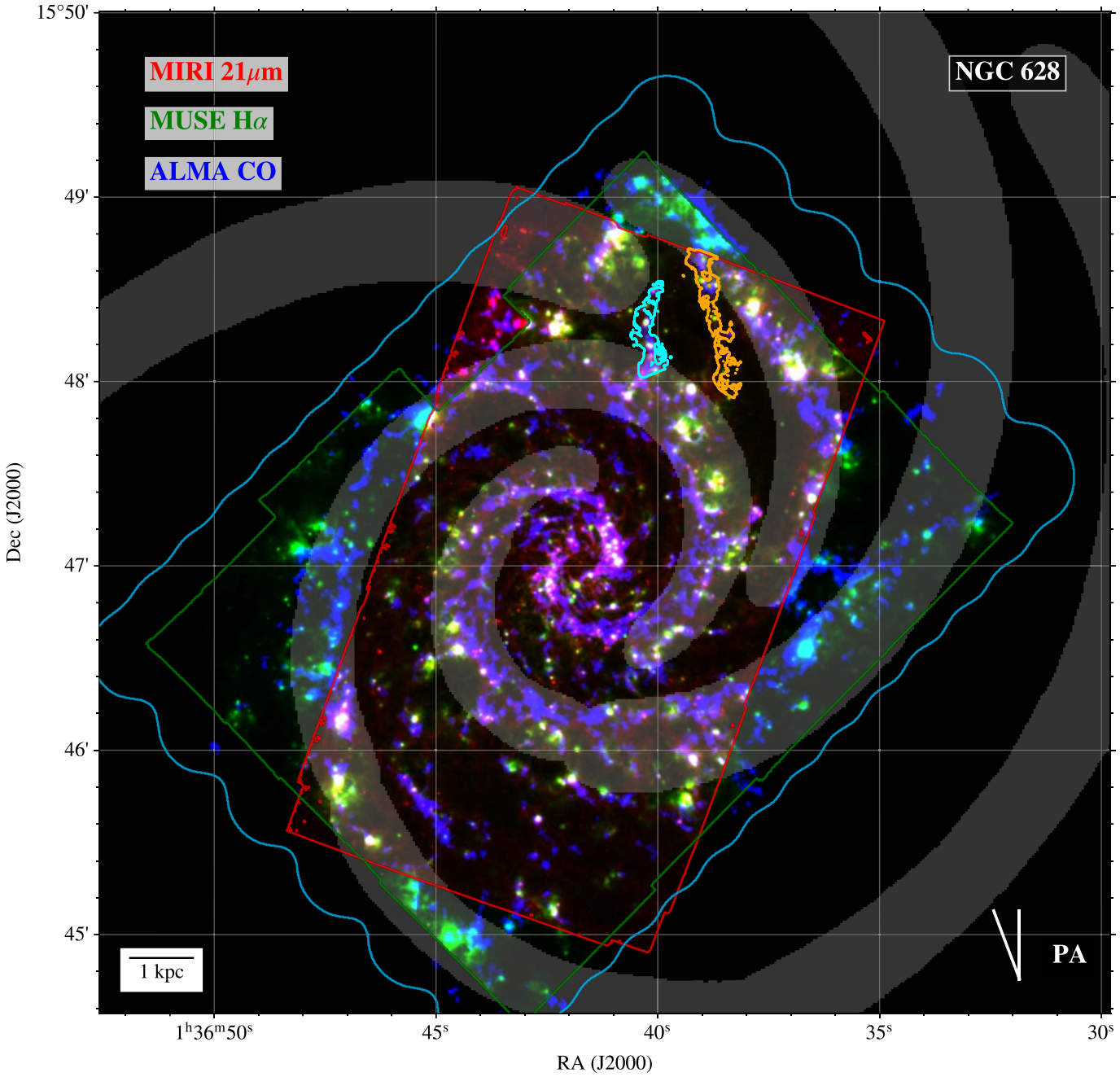

Figure 1. Three-color image of NGC 628, with ALMA CO in blue, MUSE Hα in green, and JWST 21 μm in red. The blue, red, and green boxes show the extent of each corresponding observation. The two spurs we focus on are shown as cyan (CO-rich), and orange (CO-poor) contours (see Section 3). Also shown are the spiral arms from the environmental mask, in gray. The position angle (21°; corresponding to $\theta = 0°$ in Figure 3) is indicated in the lower right, and a 1 kpc scalebar is shown in the lower left.

Leroy et al. 2012; Boquien et al. 2014). In red, we show 21 μm JWST data (Lee et al. 2022), with a resolution of 0.″67 and a surface brightness sensitivity of around 0.3 MJy sr^{-1}. In star-forming regions, this wavelength traces young, highly embedded star formation (see, e.g., radiative transfer models by De Looze et al. 2014; Williams et al. 2019), with an emitting timescale in the star-forming regions of 10 Myr for NGC 628 (Kim et al. 2022). Finally, we overlay spiral arms as defined by Querejeta et al. (2021) in gray, based on Spitzer 3.6 μm imaging, which traces the spiral arms from the old stars.

3. Spur Offset and Timescale

In Figure 3, we perform a polar (i.e., r, θ space) remapping (i.e., deprojection and derotation) of Figure 1. Here, 0° corresponds to the position angle of the galaxy shown in Figure 1, with θ increasing in a clockwise direction. In this polar projection, the spiral arms appear as nearly straight lines (these are well described as log-spirals in Querejeta et al. (2021), but the difference here is minor), and the spurs off the arms become more clear. There is also a clear offset between these three tracers in the spiral arms, as a consequence of the

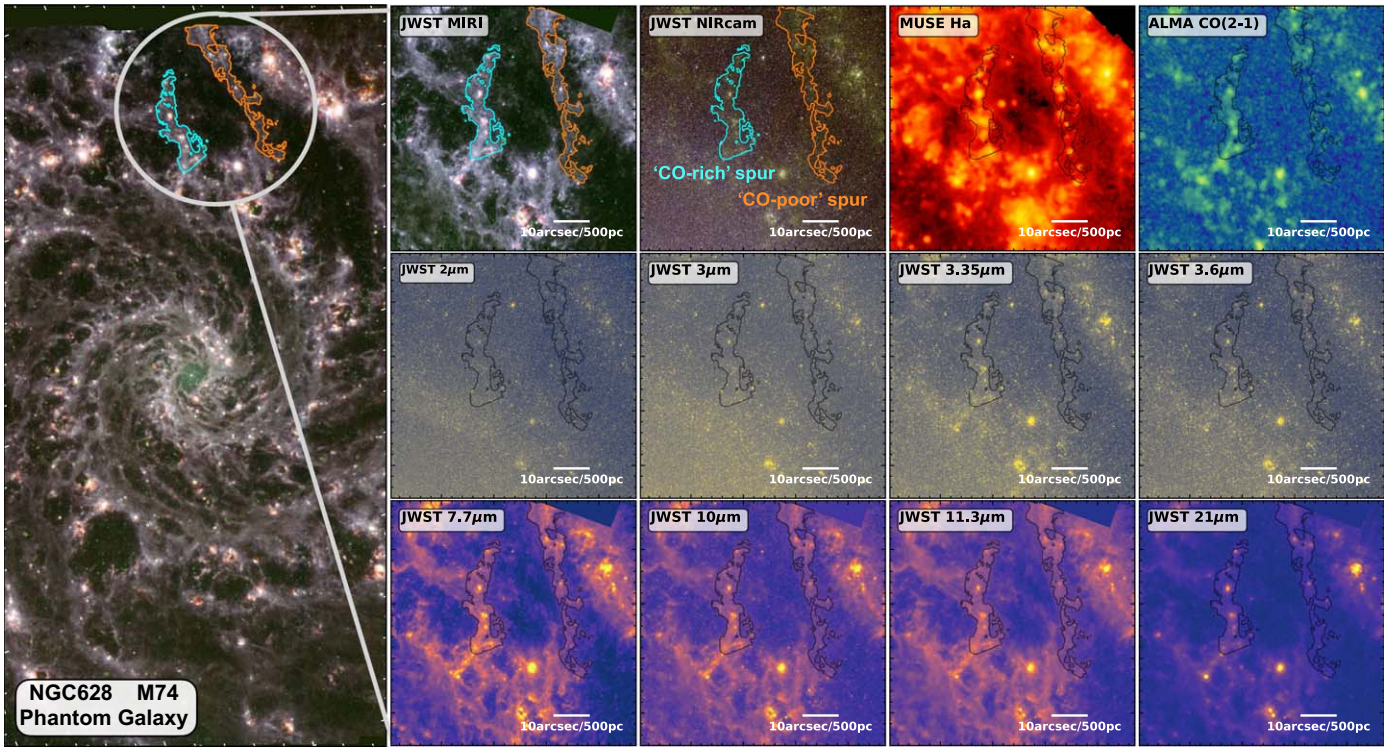

Figure 2. A holistic overview of the spurs analyzed in this study. Left: three-color image of NGC628 produced from the 770W (blue), 1000W (green), and 1130W (red) band filters from the JWST (Lee et al. 2022), and overlaid in orange is the continuum subtracted HST-Hα, with CO-rich and CO-poor spur (see Section 3) highlighted in cyan and orange, respectively. Right, top row: from left to right, three-color MIRI (same as left panel) and NIRCam (red: 200W, green: 300M, blue: 335M) zooms of the spurs, as well as MUSE Hα and ALMA CO. Right, middle: from left to right, increasing JWST NIRCam wavelengths, showing the stellar light. Right, bottom: from left to right, increasing JWST MIRI wavelengths, showing the ISM emission.

spiral pattern (e.g., Egusa et al. 2009; Kreckel et al. 2018). This is not a focus of this paper, but we note that the high resolution now available with these tracers may be useful for future direct measurements of spiral pattern speeds. There is a significant amount of CO, Hα, and 21 μm emission in spurs off the spiral arms, which is visible off all the spiral arms in Figure 1.

We will focus on two spurs in particular, both between a (deprojected) galactocentric radius of 3–4 kpc. These spurs are present near corotation (Williams et al. 2021), implying the drift times from the spiral arm will be quite long. The first has a maximum offset from the spiral arm of $\theta \simeq 40°$, and has clearly associated CO, Hα, and 21 μm emission. We will refer to this as the "CO-rich" spur. The second has a maximum offset from the spiral arm of $\theta \simeq 55°$, and is well detected in Hα and 21 μm but has no associated emission in the "strict mask" (i.e., a high-confidence, but lower-completeness mask; see Leroy et al. 2021a for details) CO moment 0 image (shown in Figure 1, although it is barely detected in the "broad mask" moment 0, which has lower confidence but higher completeness as compared to the strict mask, and is not shown here, but see Leroy et al. 2021a). Both of these spurs are also clearly detected in the other MIRI (7.7, 10, and 11.3 μm) bands, and the emission is coincident with that at 21 μm. We have selected these two as a test case, as they are neighboring spurs but quite different in their interstellar medium (ISM) composition. We reserve a more thorough cataloging and study of spurs for future work with the larger PHANGS-JWST sample.

The total 21 μm flux outside the spiral arms as defined by the environmental mask (excluding the central 1.2 kpc diameter region based on photometric decomposition by Salo et al. (2015), where disentangling the spiral arms from any potential stellar bulge or nuclear component is difficult) is around 60%, indicating a nonnegligible amount of star formation outside the spiral arms. We caution that the environmental mask is defined by Spitzer data and the gas and stellar spiral arms may not necessarily coincide. However, the spiral arm width follows an empirical definition based on the CO emission, to attempt to overcome this (Querejeta et al. 2021). There also may be a significant amount of diffuse emission at 21 μm flux, that is unlikely to originate from star formation (Leroy et al. 2022). In this sense, the percentage is likely an upper limit to the amount of 21 μm flux that can be ascribed to star formation.

We next investigate how the flux profiles of the CO, Hα, and 21 μm vary with galactocentric radius along these two spurs, to better understand the role the spiral arms have in enhancing the SFR and star formation efficiency (SFE; SFR per unit molecular gas mass). Using the spur contour in Figure 1 as a mask, we calculate radial profiles of the intensity of the three tracers for the two spurs. We use Balmer decrement-corrected Hα as a proxy for the SFR, and also calculate the profile for SFE (i.e., corrected Hα/CO). We show the profiles in Figure 4. Between the spiral arms, the SFR appears to be relatively constant, arguing against the idea of an evolutionary sequence with stars further out in the spurs being formed at an early time to those closer to the spiral arm. However, there is an increase toward the spiral arms—the inner arm for the CO-rich spur, and the outer for the CO-poor. This agrees with simulations showing that the spiral arms act to concentrate star-forming regions, leading to an overall increase in the SFR surface density (e.g., Kim et al. 2020). Yet, comparing the 21 μm and Hα to that of the CO, we see a good correspondence between the profiles, with the tracers tending to upturn at the same radii.

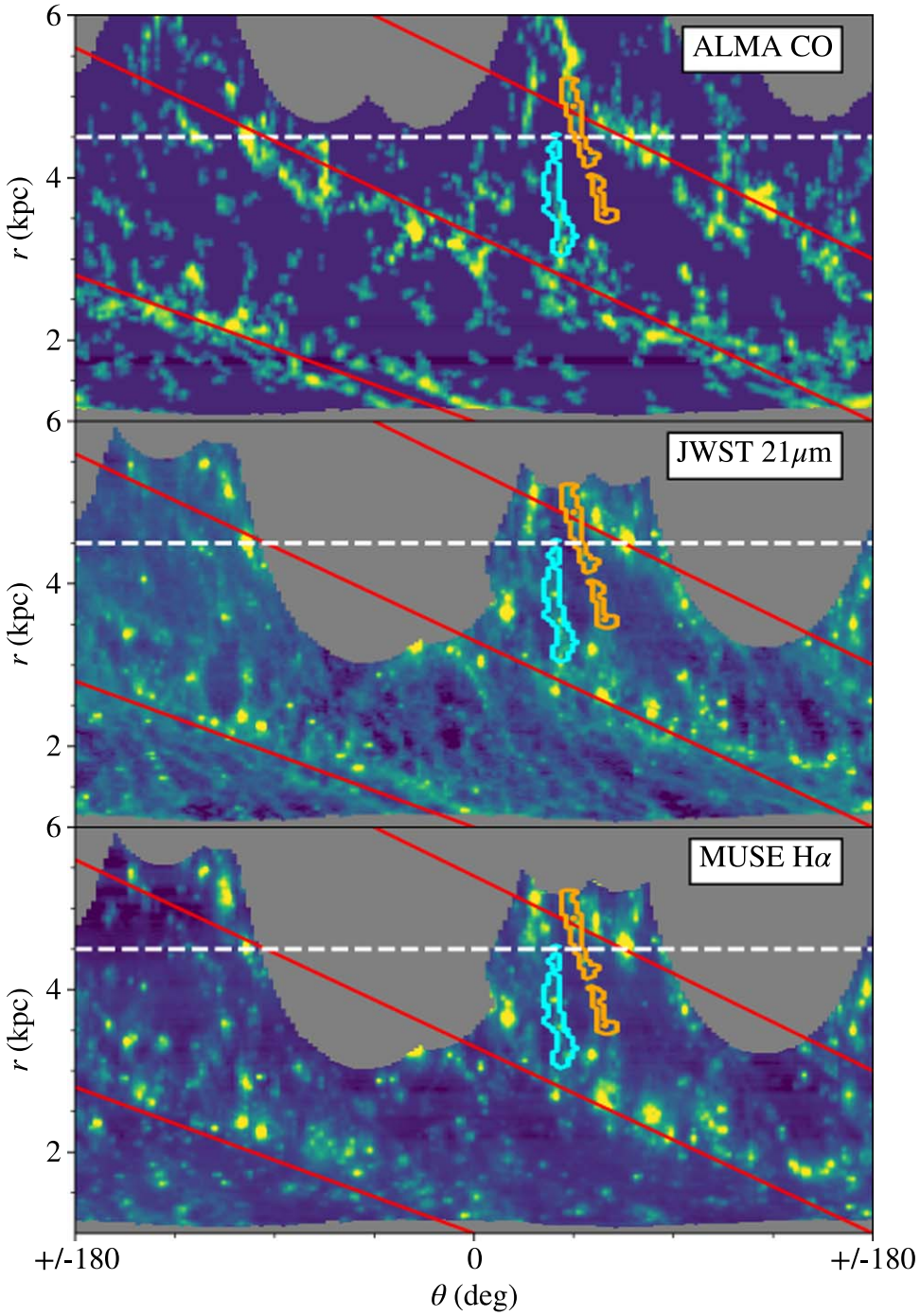

Figure 3. Polar deprojection of NGC 628 in CO (top), 21 μm (middle), and MUSE Hα (bottom). 0° is defined as the position angle (see Figure 1), and θ increases from left to right. The nominal corotation radius from Williams et al. (2021) is shown as a horizontal dashed white line. We show the approximate ridge of three spiral arms as red lines (determined from the CO). We note there is a clear offset between this CO ridge and the 21 μm/Hα ridges (see also, e.g., Kreckel et al. 2018) The cyan contour indicates the "CO-rich" spur, and the orange the "CO-poor" spur.

Indeed, the SFE profile bears this out—the SFE sometimes shows strong variation along the spurs, but the increases in SFE are localized and do not correlate with the spiral arm positions (although there is a slight increase toward the outer spiral arm in the case of the CO-poor spur). Taken together, these results advocate that the spiral arms gather together gas and star-forming regions, but have little impact on how efficiently stars are being formed, as seen in larger (but lower-resolution) samples (Querejeta et al. 2021) or in simulations (e.g., Dobbs et al. 2015).

We estimate the timescale for both of these features to appear, assuming they have drifted from the spiral arm with the passage of the density wave and at the same pattern speed. Following Egusa et al. (2009) we compute the timescale required for this spiral arm offset to occur (neglecting any noncircular motion), as

$$t = 76.8\ \mathrm{Myr}\left(\frac{\Delta\theta}{45°}\right)\left(\frac{\Omega(r) - \Omega_P}{10\ \mathrm{km\ s^{-1}\ kpc^{-1}}}\right)^{-1}, \quad (1)$$

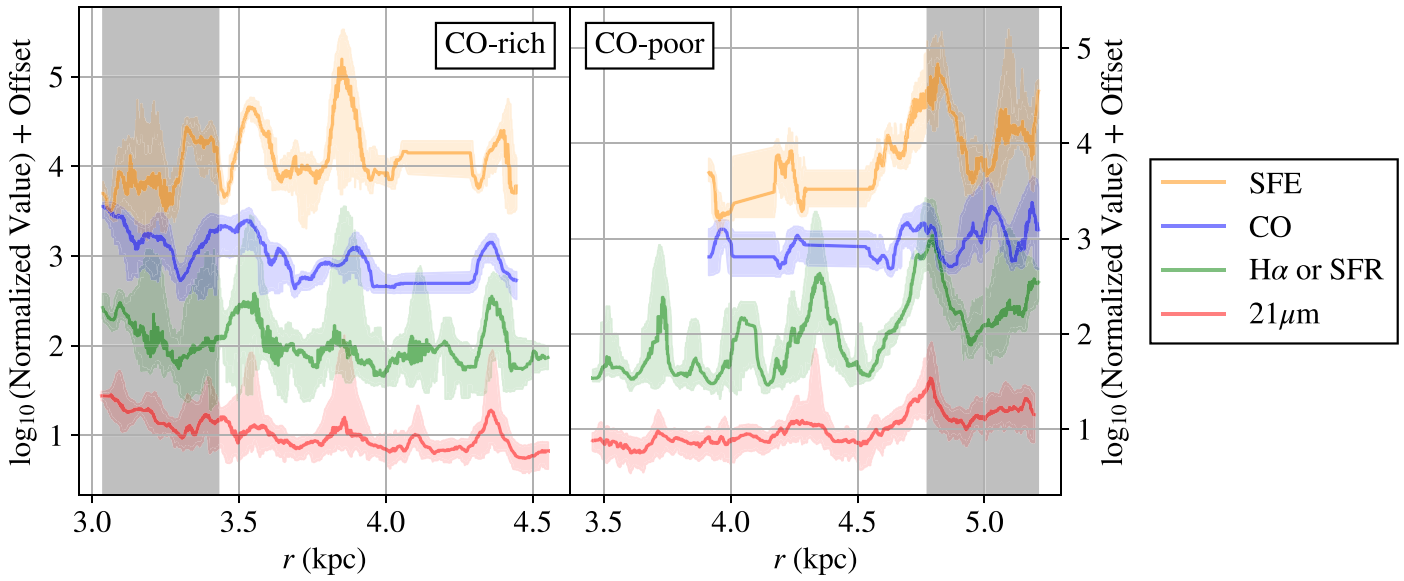

Figure 4. Profiles of 21 μm, Balmer-corrected Hα (equivalent to SFR), CO, and SFE values across the CO-rich and CO-poor spurs (the mask generated from the contours in Figure 1) as a function of galactocentric radius. The solid line shows the rolling median of the data, and the shaded regions the 16th and 84th percentiles. Each intensity is normalized by its 50th percentile value within the spur mask, and is offset for visual clarity. The shaded gray region indicates the parts of the spur within the spiral arm mask. For reference, the offsets are 1, 2, 3, and 4 for 21 μm, SFR, CO, and SFE, respectively. These lines correspond to the median value of 1.6 MJy sr^{-1} (21 μm), 5.3 $\times$ 10$^{-3}M_{\odot}$ kpc^{-2} (SFR surface density, assuming a Calzetti et al. 2007 conversion factor), 4.7 K km s^{-1} (CO), and 3.4 $\times$ 10^{-7} yr^{-1} (SFE) for the CO-rich spur, and 1.2 MJy sr^{-1}, 4.2 $\times$ 10$^{-3}M_{\odot}$ kpc^{-2}, 3.7 K kms^{-1}, and 3.3$\times$ 10^{-7} yr^{-1} for the CO-poor spur.

where Ω is the angular rotation velocity, Ω_P the pattern speed (both in kilometers per second per kiloparsec), $\Delta\theta$ the offset in degrees (i.e., the distance from spiral arm to spur along the x-axis in Figure 3, and will vary from 0 where the spur meets the spiral arm to some maximum offset), and t the timescale in units of Myr. We use $\Omega_P = 31.1^{+4.0}_{-2.9}$ km s^{-1} kpc^{-1} from Williams et al. (2021). This is a conservative value, as, for example, gravity will act to pull the gas back toward the spiral arm, lengthening the timescales. We obtain $\Omega(r)$ from the measured rotation curves in Lang et al. (2020), which vary from around 36 to 39 km s^{-1} kpc^{-1}. We estimate the maximum spur offset from Figure 3, and assume it varies linearly (as the spurs are mostly vertical in the polar projection) with r up to a maximum offset at a galactocentric radius of 4 kpc. We assign a relatively conservative uncertainty to these values of 5°.

The calculated timescales are shown in Figure 5, and are indeed quite long, as expected. These numbers are also likely lower bounds, as processes like gravitational attraction toward to spiral arm ridge will only serve to make these timescales longer. We see that the values range from close to 0 at the point where the spur joins the spiral arm up to more than 100 Myr at the farthest extent of the spur, significantly longer than the timescale we would expect the Hα and 21 μm emission to be visible for, if star formation was initiated in the arms (<10 Myr; see Section 2). The same conclusion was found by Schinnerer et al. (2017) in M51, perhaps indicating that this is a general result within galaxies. Altogether, our analysis suggests that stars can form in situ within spurs, rather than moving from the spiral arms. This has been seen in some recent simulations (e.g., Smith 2020; Treß et al. 2021), and combined with results showing the star formation efficiency may not be higher in the spiral arms (e.g., Ragan et al. 2018; Querejeta et al. 2021), these results point toward a picture where the spiral arms merely gather gas together, rather than being instrumental in causing the onset of star formation.

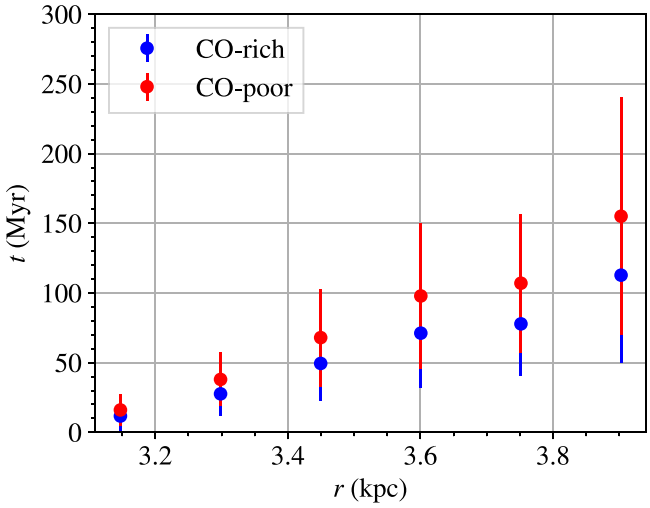

Figure 5. Offset timescale (see Equation (1)) as a function of galactocentric radius for the CO-rich (blue) and CO-poor (red) spurs, calculated between a galactocentric radius of 3 and 4 kpc.

The fact that one of these spurs is rich in CO and the other poor is also intriguing, given their close proximity. It seems possible that these spurs could potentially be forming from superbubble expansion (Kim et al. 2020), as these spurs are on the edge of one of the large bubbles cataloged in Barnes et al. (2022) and Watkins et al. (2022), and so should be in roughly the same evolutionary state. Perhaps, then, some feedback mechanisms have been more efficient at destroying gas in one spur compared to the other, or maybe the CO-poor one is older. This could be addressed both by observing the coincidence of spurs and bubbles, and using stellar clusters from combined Hubble Space Telescope (HST) JWST observations as "clocks." This is beyond the scope of this work, but would be an interesting future study with a full PHANGS-JWST sample of spurs, bubbles, and stellar clusters.

4. Conclusions

In this Letter, we have combined ALMA, VLT-MUSE, and new JWST observations in the context of the PHANGS collaboration to examine the youngest, highly embedded stage of star formation in a CO-rich and CO-poor spur off the prominent northern spiral arm of NGC 628. These were chosen as a test case, as they are next to each other but clearly quite different in their ISM composition. Both of these spurs show an increase in star formation toward spiral arms, but little indication of an increase in the star formation efficiency. Given the angular offset of these spurs, assuming they are formed on the arm and drifted off due to the difference between circular rotation speed and arm pattern speed, we infer a timescale of around 100 Myr or more, 1 order of magnitude higher than the timescales of the Hα and 21 μm emission (Kim et al. 2021, 2022). These results imply that stars are forming in situ within the spurs, rather than being produced within the spiral arms and then traveling there.

This work represents an initial exploration into how JWST observations will redefine our view of the earliest phases of galactic-scale star formation, and how this affects the structure of the ISM and the process of star formation in different environments. In particular, combining a spur catalog with both exposed (measured from HST) and embedded (measured from JWST) stellar clusters will help to understand the evolutionary sequence of the structure of the ISM (e.g., Chandar et al. 2017). With the full 19 galaxies of the PHANGS-JWST sample, we will be able to form a new picture of the highly complex, filamentary nature of the ISM.

The authors would like to thank the anonymous referee for constructive comments, which have improved this manuscript. T.G.W. would also like to thank David Williams, for everything over the years. This work was carried out as part of the PHANGS collaboration. The analysis scripts underlying this work are available at https://github.com/thomaswilliamsastro/jwst_ngc628. All the JWST data used in this paper can be found in MAST doi:10.17909/436y-rd76.

This work is based on observations made with the NASA/ESA/CSA JWST. The data were obtained from the Mikulski Archive for Space Telescopes at the Space Telescope Science Institute, which is operated by the Association of Universities for Research in Astronomy, Inc., under NASA contract NAS 5-03127. The observations are associated with JWST program 2107. Based on observations collected at the European Southern Observatory under ESO programs 094.C-0623 (PI: Kreckel), 095.C-0473, 098.C-0484 (PI: Blanc), and 1100.B-0651 (PHANGS-MUSE; PI: Schinnerer), as well as 094.B-0321 (MAGNUM; PI: Marconi), 099.B-0242, 0100.B-0116, 098.B-0551 (MAD; PI: Carollo), and 097.B-0640 (TIMER; PI: Gadotti). This paper makes use of the following ALMA data: ADS/JAO.ALMA#2012.1.00650.S. ALMA is a partnership of ESO (representing its member states), NSF (USA) and NINS (Japan), together with NRC (Canada), MOST and ASIAA (Taiwan), and KASI (Republic of Korea), in cooperation with the Republic of Chile. The Joint ALMA Observatory is operated by ESO, AUI/NRAO and NAOJ.

T.G.W. and E.S. acknowledge funding from the European Research Council (ERC) under the European Union's Horizon 2020 research and innovation program (grant agreement No. 694343). J.S. acknowledges the support of the Natural Sciences and Engineering Research Council of Canada (NSERC) through a Canadian Institute for Theoretical Astrophysics (CITA) National Fellowship. J.M.D.K. gratefully acknowledges funding from ERC via the ERC Starting Grant "MUSTANG" (grant agreement No. 714907). COOL Research DAO is a Decentralized Autonomous Organization supporting research in astrophysics aimed at uncovering our cosmic origins. J.Pe. acknowledges support by the DAOISM grant ANR-21-CE31-0010 and by the Programme National "Physique et Chimie du Milieu Interstellaire" (PCMI) of CNRS/INSU with INC/INP, co-funded by CEA and CNES. M.C. gratefully acknowledges funding from the Deutsche Forschungsgemeinschaft (DFG) through an Emmy Noether Research Group (grant No. CH2137/1-1). M.B. acknowledges support from FONDECYT regular grant 1211000 and by the ANID BASAL project FB210003. E.J.W., R.S.K., S.C.O.G., and M.C.S acknowledge funding from DFG via the Collaborative Research Center "The Milky Way System" (SFB 881, funding ID 138713538, subprojects A1, B1, B2, B8, and P1). K.K. and O.E. gratefully acknowledge funding from DFG in the form of an Emmy Noether Research Group (grant No. KR4598/2-1, PI Kreckel). F.B. would like to acknowledge funding from ERC via the ERC Consolidator Grant "Empire" (grant agreement No. 726384). J.K. gratefully acknowledges funding from DFG through the DFG Sachbeihilfe (grant No. KR4801/2-1). E.R. acknowledges the support of the Natural Sciences and Engineering Research Council of Canada (NSERC), funding reference No. RGPIN-2022-03499. R.S.K. and S.C.O.G. acknowledge support from ERC via the ERC Synergy Grant "ECOGAL" (project ID 855130) and from the Heidelberg Cluster of Excellence (EXC 2181-390900948) "STRUCTURES," funded by the German Excellence Strategy. R.S.K. also thanks the German Ministry for Economic Affairs and Climate Action for funding in project "MAINN" (funding ID 50OO2206). M.Q. acknowledges support from the Spanish grant PID2019-106027GA-C44, funded by MCIN/AEI/10.13039/501100011033. K.G. is supported by the Australian Research Council through the Discovery Early Career Researcher Award (DECRA) Fellowship DE220100766 funded by the Australian Government. A.K.L. gratefully acknowledges support by grants 1653300 and 2205628 from the National Science Foundation, by award JWST-GO-02107.009-A, and by a Humboldt Research Award from the Alexander von Humboldt Foundation. G.A.B. acknowledges the support from ANID Basal project FB210003.

Facilities: JWST, ALMA, VLT-MUSE.

Software: astropy (Astropy Collaboration et al. 2013, 2018), numpy (Harris et al. 2020), scipy (Virtanen et al. 2020), scikit-image (Van der Walt et al. 2014), matplotlib (Hunter 2007), uncertainties (http://pythonhosted.org/uncertainties/).

ORCID iDs

Thomas G. Williams https://orcid.org/0000-0002-0012-2142
Jiayi Sun https://orcid.org/0000-0003-0378-4667
Ashley T. Barnes https://orcid.org/0000-0003-0410-4504
Eva Schinnerer https://orcid.org/0000-0002-3933-7677
Jonathan D. Henshaw https://orcid.org/0000-0001-9656-7682
Sharon E. Meidt https://orcid.org/0000-0002-6118-4048
Miguel Querejeta https://orcid.org/0000-0002-0472-1011
Elizabeth J. Watkins https://orcid.org/0000-0002-7365-5791

Frank Bigiel https://orcid.org/0000-0003-0166-9745
Guillermo A. Blanc https://orcid.org/0000-0003-4218-3944
Médéric Boquien https://orcid.org/0000-0003-0946-6176
Yixian Cao https://orcid.org/0000-0001-5301-1326
Mélanie Chevance https://orcid.org/0000-0002-5635-5180
Oleg V. Egorov https://orcid.org/0000-0002-4755-118X
Eric Emsellem https://orcid.org/0000-0002-6155-7166
Simon C. O. Glover https://orcid.org/0000-0001-6708-1317
Kathryn Grasha https://orcid.org/0000-0002-3247-5321
Hamid Hassani https://orcid.org/0000-0002-8806-6308
Sarah Jeffreson https://orcid.org/0000-0002-4232-0200
María J. Jiménez-Donaire https://orcid.org/0000-0002-9165-8080
Jaeyeon Kim https://orcid.org/0000-0002-0432-6847
Ralf S. Klessen https://orcid.org/0000-0002-0560-3172
Kathryn Kreckel https://orcid.org/0000-0001-6551-3091
J. M. Diederik Kruijssen https://orcid.org/0000-0002-8804-0212
Kirsten L. Larson https://orcid.org/0000-0003-3917-6460
Adam K. Leroy https://orcid.org/0000-0002-2545-1700
Daizhong Liu https://orcid.org/0000-0001-9773-7479
Ismael Pessa https://orcid.org/0000-0002-0873-5744
Jérôme Pety https://orcid.org/0000-0003-3061-6546
Francesca Pinna https://orcid.org/0000-0001-5965-3530
Erik Rosolowsky https://orcid.org/0000-0002-5204-2259
Karin M. Sandstrom https://orcid.org/0000-0002-4378-8534
Rowan Smith https://orcid.org/0000-0002-0820-1814
Mattia C. Sormani https://orcid.org/0000-0001-6113-6241
Sophia Stuber https://orcid.org/0000-0002-9333-387X
David A. Thilker https://orcid.org/0000-0002-8528-7340
Bradley C. Whitmore https://orcid.org/0000-0002-3784-7032

References

Anand, G. S., Lee, J. C., Van Dyk, S. D., et al. 2021a, MNRAS, 501, 3621
Anand, G. S., Rizzi, L., Tully, R. B., et al. 2021b, AJ, 162, 80
Astropy Collaboration, Price-Whelan, A. M., Sipőcz, B. M., et al. 2018, AJ, 156, 123
Astropy Collaboration, Robitaille, T. P., Tollerud, E. J., et al. 2013, A&A, 558, A33
Barnes, A. T., Watkins, E. J., Meidt, S. E., et al. 2022, arXiv:2212.00812
Boquien, M., Buat, V., & Perret, V. 2014, A&A, 571, A72
Calzetti, D., Kennicutt, R. C., Engelbracht, C. W., et al. 2007, ApJ, 666, 870
Chandar, R., Chien, L. H., Meidt, S., et al. 2017, ApJ, 845, 78
Chevance, M., Krumholz, M. R., McLeod, A. F., et al. 2022, arXiv:2203.09570
Chevance, M., Kruijssen, J. M. D., Vazquez-Semadeni, E., et al. 2020, SSRv, 216, 50
Corder, S., Sheth, K., Scoville, N. Z., et al. 2008, ApJ, 689, 148
De Looze, I., Fritz, J., Baes, M., et al. 2014, A&A, 571, A69
Dobbs, C., & Baba, J. 2014, PASA, 31, e035
Dobbs, C. L., & Bonnell, I. A. 2006, MNRAS, 367, 873
Dobbs, C. L., & Pringle, J. E. 2010, MNRAS, 409, 396
Dobbs, C. L., Pringle, J. E., & Duarte-Cabral, A. 2015, MNRAS, 446, 3608
Egusa, F., Kohno, K., Sofue, Y., Nakanishi, H., & Komugi, S. 2009, ApJ, 697, 1870
Elmegreen, B. G. 2007, ApJ, 668, 1064
Emsellem, E., Schinnerer, E., Santoro, F., et al. 2022, A&A, 659, A191
Fukui, Y., Habe, A., Inoue, T., Enokiya, R., & Tachihara, K. 2021, PASJ, 73, S1
Harris, C. R., Millman, K. J., van der Walt, S. J., et al. 2020, Natur, 585, 357
Hunter, J. D. 2007, CSE, 9, 90
Kennicutt, R. C. J. 1998, ARA&A, 36, 189
Kennicutt, R. C., & Evans, N. J. 2012, ARA&A, 50, 531
Kim, J., Chevance, M., Kruijssen, J. M. D., et al. 2021, MNRAS, 504, 487
Kim, J., Chevance, M., Kruijssen, J., et al. 2022, arXiv:2211.15698
Kim, W.-T., Kim, C.-G., & Ostriker, E. C. 2020, ApJ, 898, 35
Kim, W.-T., & Ostriker, E. C. 2006, ApJ, 646, 213
Koda, J., Scoville, N., Sawada, T., et al. 2009, ApJL, 700, L132
Kreckel, K., Faesi, C., Kruijssen, J. M. D., et al. 2018, ApJL, 863, L21
La Vigne, M. A., Vogel, S. N., & Ostriker, E. C. 2006, ApJ, 650, 818
Lang, P., Meidt, S. E., Rosolowsky, E., et al. 2020, ApJ, 897, 122
Lee, J. C., Sandstrom, K. M., Leroy, A. K., et al. 2022, arXiv:2212.02667
Leroy, A. K., Bigiel, F., de Blok, W. J. G., et al. 2012, AJ, 144, 3
Leroy, A. K., Hughes, A., Liu, D., et al. 2021a, ApJS, 255, 19
Leroy, A. K., Schinnerer, E., Hughes, A., et al. 2021b, ApJS, 257, 43
Leroy, A. K., Sandstrom, K. M., Rosolowsky, E., et al. 2022, ApJL, submitted
Longmore, S. N., Kruijssen, J. M. D., Bastian, N., et al. 2014, in Protostars and Planets VI, ed. H. Beuther et al. (Tucson, AZ: Univ. of Arizona Press), 291
Louie, M., Koda, J., & Egusa, F. 2013, ApJ, 763, 94
Mandowara, Y., Sormani, M. C., Sobacchi, E., & Klessen, R. S. 2022, MNRAS, 513, 5052
McQuinn, K. B. W., Skillman, E. D., Dolphin, A. E., Berg, D., & Kennicutt, R. 2017, AJ, 154, 51
Morgan, W. W., Whitford, A. E., & Code, A. D. 1953, ApJ, 118, 318
Moustakas, J., Kennicutt, R. C. J., & Tremonti, C. A. 2006, ApJ, 642, 775
Oey, M. S., & Clarke, C. J. 1997, MNRAS, 289, 570
Querejeta, M., Schinnerer, E., Meidt, S., et al. 2021, A&A, 656, A133
Ragan, S. E., Moore, T. J. T., Eden, D. J., et al. 2018, MNRAS, 479, 2361
Rieke, G. H., Young, E. T., Engelbracht, C. W., et al. 2004, ApJS, 154, 25
Roberts, W. W. 1969, ApJ, 158, 123
Salo, H., Laurikainen, E., Laine, J., et al. 2015, ApJS, 219, 4
Schinnerer, E., Meidt, S. E., Colombo, D., et al. 2017, ApJ, 836, 62
Smith, R. J., Treß, R. G., Sormani, M. C., et al. 2020, MNRAS, 492, 1594
Stuber, S. K., Schinnerer, E., Thomas, T. G., et al. 2022, A&A, submitted
Tan, J. C. 2000, ApJ, 536, 173
Treß, R. G., Sormani, M. C., Smith, R. J., et al. 2021, MNRAS, 505, 5438
Van der Walt, S., Schönberger, J. L., Nunez-Iglesias, J., et al. 2014, PeerJ, 2, e453
Virtanen, P., Gommers, R., Oliphant, T. E., et al. 2020, NatMe, 17, 261
Wada, K., & Koda, J. 2004, MNRAS, 349, 270
Watkins, E. J., Barnes, A., Henny, K. F., et al. 2022, arXiv:2212.00811
Williams, T. G., Baes, M., De Looze, I., et al. 2019, MNRAS, 487, 2753
Williams, T. G., Schinnerer, E., Emsellem, E., et al. 2021, AJ, 161, 185